KSME International Journal Vol. 11, No. 2, pp. 125~135, 1997

Prediction of Fatigue Strength in HSS-Co, S55C and the Friction Welded Materials Based on Statistical Evaluation of Inclusion Size

Chang-Min Suh* and Duck-Young Suh**

(Received February 12, 1996)

In this paper, the effects of nonmetallic inclusions on the fatigue strength of medium and high strength steels are quantitatively investigated by considering the relationship between the Vickers hardness, Hv and the maximum size of nonmetallic inclusion, $\sqrt{(area)_{max}}$. The maximum size of nonmetallic inclusion defined by the square root of the projected area in an inclusion can be estimated by the statistics of extreme values with a definite number of specimens or structural components. While most of other studies using the parameter $\sqrt{(area)_{max}}$ have performed the experiments with the specimens with small artificial defects or notches, this study investigates the possibility of prediction on fatigue strength in the unnotched smooth specimens. The results show that strength of the friction welded joints of HSS-Co to S55C carbon steel is almost equal to that of the weaker material in the optimum welding conditions. Under the limiting condition for the nonpropagating cracks emanating from defects or inclusions, the threshold stress intensity factor range ΔK_{th} and the lower limit of fatigue strength σ_{wl} were successfully estimated from the largest inclusion size $\sqrt{(area)_{max}}$. From the analysis of SEM fractographs, it can be concluded that the fatigue fractures of the specimens are associated primarily with the inclusions located at the outer periphery of the specimens.

Key Words: Friction Welding (FRW), Maximum Size of Nonmetallic Inclusion, Vickers Hardness, Statistics of Extreme Values, Fatigue Limit, Threshold Value of Stress Intensity Factor Range, SEM Fractograph

1. Introduction

The friction welding (FRW) of HSS-Co (the special tool steel equivalent of SKH56) to S55C carbon steel is used as a process for joining dissimilar materials in such mechanical parts as the automotive industry for the purpose of cost reduction of manufacturing economy, and has advantages in respect of simplicity and efficiency to productivity.

The effect of certain nonmetallic inclusions on fatigue crack initiation in a specimen or component has been well established (Atkinson, 1960; Ineson et al., 1956; Thornton, 1971; Murakami et al., 1991; Fowler, 1979) and Lankford, 1977). The role of nonmetallic inclusions in steel has received increasing attention, much having been written on the topics in recent years (Thornton, 1971; Fowler, 1979; Murakami et al., 1987, 1989a, and 1989b; Toriyama et al., 1991; and Murakami, 1993).

Several methods of inclusion counting exist. The Fox and Fairey inclusion counts showed the need for a quantitative assessment of inclusions, although these counts were in fact shown not to be strictly quantitative (Atkinson, 1960). These studies have shown qualitatively that nonmetallic

* Department of Mechanical Engineering, Kyungpook National University
** Department of Heat-Refrigeration Engineering, Doowon Technical College

inclusions are responsible for this fatigue behavior of high strength steels (Atkinson, 1960; Ineson et al., 1956; De Kazinczy, 1970 and Dieter, 1976). Inclusions are assumed to be detrimental to the mechanical properties of steel, but there has been little evidence of any direct relationship between nonmetallic content and fatigue properties.

In general, fatigue resistance is one of the most sensitive properties to the influence of inclusions, and high tensile strength steels are most susceptible in this respect. However, the relationship has proved to be elusive owing to the difficulties of measuring and analyzing all the factors. That is, inclusion size, shape, distribution, interfacial strength and physical properties relative to the matrix must be considered when evaluating their effect on fatigue initiation. Therefore, the microscopic mechanism of fatigue crack initiation at inclusions has been investigated by several researchers (Lankford, 1977 and De Kazinczy, 1970) as well as by statistical analysis of the effects of the nonmetallic inclusion distribution on the fatigue strength (Murakami, 1987) and also a fracture mechanics approach to inclusion problems (Lankford, 1977). However, most of these studies do not lead to a successful prediction of the fatigue strength because of a large scatter.

Recently, Murakami et al. (1993) has established the methodology for the quantitative evaluation of the effects of small defects on the fatigue strength of various steels. And the methodology has been extended to predict the fatigue strength influenced by inclusions (Murakami et al., 1987 and 1989a).

In this study, the quantitative assessment of the effects of nonmetallic inclusions on fatigue strength in the unnotched smooth specimens has been analyzed using the prediction equation that was proposed by Murakami et al. based on statistical evaluation of inclusion size. It is shown that the fatigue strength of materials containing inclusions larger than a critical size can be predicted by the Vickers hardness (Hv) for medium or high strength steels (Dieter, 1976) and the square root of the projection area of the inclusion, $\sqrt{(area)_{max}}$ regardless of the shape.

And it is possible to predict the upper (σ_{wu}) and lower limits (σ_{wl}) of the fatigue strength from the hardness (Hv) of a matrix and the maximum size of inclusions ($\sqrt{(area)_{max}}$). The expected value of $\sqrt{(area)_{max}}$ in a definite number of specimens can be estimated by the statistics of extreme values (Toriyama et al., 1991; Murakami et al., 1989b; Murakami, 1993 and Vemura et al., 1990). All data obtained are discussed systematically with the prediction equation of fatigue strength (Murakami et al., 1987, 1989a and 1991).

2. Experimental and Quantitative Evaluation Procedures

2.1 Preparation of specimens

In the previous papers (Suh et al., 1995a and 1995b), the authors have studied on fatigue strength of medium and high strength steels using artificially notched and smooth specimens. Although the fatigue tests were carried out under rotary bending, the statistics of extreme values (Murakami, 1993) is useful for the estimation of fatigue strength (σ_w) and the threshold stress intensity factor range (ΔK_{th}) for defects and nonmetallic inclusions contained in steels.

For the quantitative evaluation conducted in the present work, the raw materials were the commercial S55C carbon steel and HSS-Co (the special tool steel equivalent of SKH56) which intensified Co composition along with the nominal compositions of high speed steel (HSS). The chemical compositions of the HSS-Co and S55C are shown in Table 1. The mechanical properties of the raw materials have already reported the other paper (Suh et al., 1995a).

Table 1 Chemical compositions of raw materials (wt, %)

Material	C	Si	Mn	P	S	Cr	Ni	W	Mo	V	Co
HSS-Co (equivalent of SKH 56)	1.0	0.3	0.3	Max. 0.025	Max. 0.010	4.2	-	5.5	6.5	1.60	8.0
S55C	0.52~0.58	0.15~0.35	0.6~0.9	Max. 0.030	Max. 0.035	Max. 0.20	Max. 0.20	-	-	-	-

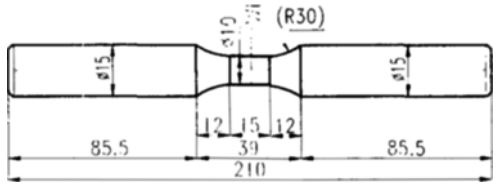

Fig. 1 Shape of smooth fatigue specimen (unit: mm)

Table 2 Friction welding conditions

Welding maerials	Rotating speed N(rpm)	Friction pressure P_1(MPa)	Upsetting pressure P_2(MPa)	Friction time t_1(sec)	Upsetting time t_2(sec)
HSS-Co to S55C	1600	39.2	196	15	3

* Welding diameter: d=18 mm

Friction welding performed by continuous friction welding machine was carried out under the appropriate welding parameters as shown in Table 2 (Suh,1995a).

The friction welded specimens were placed into the furnace during 4hrs when those had reached at 760°C and then were dealt with by anealing in order to relieve the residual stress.

Two base materials were also processed as heat treatment as the FRW specimens were done in order to compare each of the test results. The fatigue specimen was machined into the configuration shown in Fig. 1. The specimen has a total length of 210mm with ϕ 15mm and shank length of 39mm. Also, the smooth part of specimens has a length of 15mm with ϕ10mm.

The general heat treatment of HSS including 3 times tempering was done in all specimens to compare the material properties each other (Suh, 1994). And the gage sections of each specimen were manually ground with SiC paper until #1200 and cleaned with acetone prior to evaluating.

2.2 Fatigue tests

The fatigue test was performed using Ono-type rotary bending fatigue tester (H5, 98N•m, 3450 rpm) in room air. All the tests were conducted at the stress level above the fatigue limit at which the majority of the test pieces would be expected to be broken. After the fatigue tests the Vickers hardness (Hv) was checked under the weight of 200g for 30 second near the fractured surface. The hardness represented the average values of 7 points on the specimens. Table 3 shows the details of the test results (Suh et al., 1995a and 1995b).

Table 3 Results of fatigue tests

Materials	Smooth specimen No.	H_v	d (mm)	N_f ($\times 10^5$)	σ_w (MPa)
HSS-Co	1	1053	10.15	∞	763.7
	2	969	10.15	530	906.9
	3	1022	10.15	335	1002.3
	4	918	10.1	344	930.1
S55C	1	249	10.05	44	481.9
	2	250	10.08	∞	273.0
	3	251	10.10	803	319.7
	4	233	10.20	157	404.5
	5	250	9.81	215	359.5
	6	261	9.87	792	321.8
FRW (S55C side)	1	268	9.89	∞	299.0
	2	244	9.75	12.9	506.0
	3	268	9.80	74.4	424.0
	4	266	9.75	185	377.0
	5	307	9.68	∞	319.0
	6	287	9.54	81	459.9

* d : Diameter of specimen
N_f: No. of cycles to failure
σ_w: Fatigue strength

2.3 The experimental procedures

After rotary bending tests, one or both sides of the fractured surface were cut in perpendicular to the direction of maximum tensile stress in order to investigate the effects of nonmetallic inclusions on the fatigue strength of the specimens by means of the suggested procedures (Murakami, 1993). And the smooth sections of each specimen were ground (SiC paper #600~#2000) and polished (diamond paste) using the grinder/polisher (Metaserve 2000). Then etching (HSS-Co: glyceregia, S55C: 4% nital), gold coating (EMI Tech K550) and SEM study (S2700, 20KV, Hitachi) were performed in the usual sequence. Finally, the Vickers hardness was checked on the weight of 200g for 30 second using the Micro-Vickers tester (HMV 2000, Shimadzu).

3. Results and Discussion

3.1 The influence and measurement of inclusion location and size

The existence of nonmetallic inclusions causes different fatigue behaviors in all specimens and brings up the difficulty of the quantitative evaluation of fatigue strength. In general, the fatigue limit of steels is recognized as the limiting condition for the nonpropagating cracks emanating from a defect or inclusion, not as the critical condition for crack initiation. The concept of the fatigue limit is important in understanding the phenomena of fatigue fracture caused by inclusions. Considering the behaviour of cracks that originate from an inclusion, it may be reasonable to think that these cracks initiate at the interface or the interior of the inclusion of maximum size. In fatigue limit, these cracks would probably stop propagating, and the existence of inclusions is mechanically equivalent to stress-free defects. It is possible for the maximum inclusion size to contribute as a major factor affecting the fatigue strength.

The works of De Kazinczy (1970) and Murakami et al. (1987, 1989, 1989a and 1991) have indicated that inclusions of a surface or subsurface location shown in Fig. 2 do influence the fatigue failure. The initiation site of fracture in the test section empirically is located at $\sigma \geq 0.9\sigma_w$ (σ_w: fatigue strength) or the depth $h \leq 0.5d$ mm (d: specimen diameter) from the test surface. In dangerous part of the specimen section, about 20 SEM photographs for each specimen were taken, and the biggest nonmetallic inclusions every photograph were observed and recorded to investigate the maximum size of inclusion ($\sqrt{(area)_{max,j}}$, j=1~20: No. of SEM photos) defined by the square root of the projected area of an inclusion.

In determining the inclusion size, the inclusions in each photo of view were checked on the standard examined area, S_0 (HSS-Co: 0.0046mm^2, S55C: 0.0412mm^2).

Depending on the relative location of an inclusion in the free surface of a specimen shown in Fig. 2, the fatigue strength is predicted by following Eqs. (1), (2) and (3) (Murakami, 1993);

For surface inclusions,

$$\sigma_w = 1.43 \times (H_v + 120)/(\sqrt{(area)_{max}})^{1/6} \quad (1)$$

For subsurface inclusions,

$$\sigma_w = 1.41 \times (H_v + 120)/(\sqrt{(area)_{max}})^{1/6} \quad (2)$$

For interior inclusions,

$$\sigma_w = 1.56 \times (H_v + 120)/(\sqrt{(area)_{max}})^{1/6} \quad (3)$$

where, σ_w, Hv and $\sqrt{(area)_{max}}$ are measured in MPa, kg$_f$/mm^2 and μm, respectively.

Typical inclusions in steels of S55C and HSS-Co are illustrated in Figs. 3 and 4. As shown in Fig. 3, the inclusions were the spheroidal cavities exposed in cross-section of the S55C specimen. The biggest one was adopted as a maximum size of inclusion $\sqrt{(area)_{max,1}}$ in one photo. After checking the maximum inclusion size from the $\sqrt{(area)_{max,1}}$ to the $\sqrt{(area)_{max,20}}$ of the 20 SEM photos, the $\sqrt{(area)_{max}}$ for one specimen has been obtained in the usual manner by means of the statistics of extreme values to predict the fatigue strength, σ_w. According to this method, the expected value of $\sqrt{(area)_{max}}$ increases with increasing test volume or number of specimens.

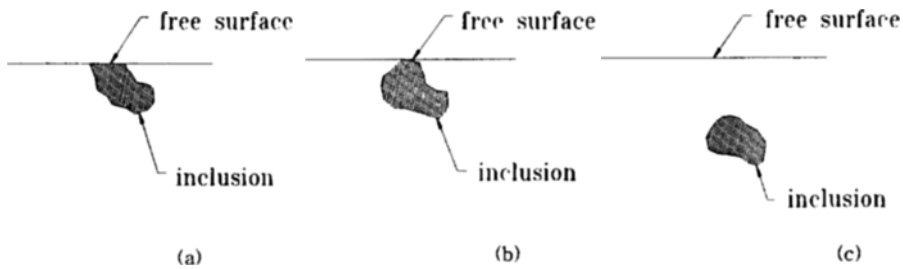

Fig. 2 Locations of (a) surface, (b) subsurface and (c) interior inclusions

Table 4 Results of the nonmetallic inclusions measured on the specimen surface using the statistics of extreme values (Murakami,1993)

Materials	$\sqrt{(area)_{max,j}}$ (μm)	j	F_j	y_j	The related equations
HSS-Co (No. 3)	3	1	4.7619	−1.1133	$F_j=\frac{j}{(n+1)}\times 100(\%)$, $y_j=-\ln[-\ln\frac{j}{(n+1)}]$
	3.9	2	9.5238	−0.8550	$a=\frac{n\cdot\sum_{j=1}^{n}(y_i\cdot\sqrt{(area)_{max,j}})-\sum_{j=1}^{n}y_j\cdot\sum_{j=1}^{n}\sqrt{(area)_{max,j}}}{n\cdot\sum_{j=1}^{n}(y_j)^2-(\sum_{j=1}^{n}y_j)^2}$
	3.9	3	14.2857	−0.6657	
	4.4	4	19.0476	−0.5057	
	4.4	5	23.8095	−0.3612	
	4.4	6	28.5714	−0.2253	
	4.4	7	33.3333	−0.0940	
	4.4	8	38.0952	0.0355	$b=\frac{\sum_{j=1}^{n}\sqrt{(area)_{max,j}}-a\cdot\sum_{j=1}^{n}y_j}{n}$
	4.4	9	42.8571	0.1657	
	5	10	47.6190	0.2984	$\sqrt{(area)_{max}}=a\cdot y_{(N)}+b$
	5	11	52.3809	0.4359	
	5.6	12	57.1428	0.5805	$h=\frac{\sum_{j=1}^{n}\sqrt{(area)_{max,j}}}{n}$, $V_0=h\cdot S_0$, $V_0=0.05\pi d^2 l$
	5.6	13	61.9047	0.7348	
	5.6	14	66.6666	0.9027	
	5.6	15	71.4285	1.0892	$T_{(N)}=\frac{V\times N}{V_0}$
	5.6	16	76.1904	1.3021	
	6.1	17	80.9523	1.5544	$y_{(N)}=\ln[-\ln\frac{T_{(N)}-1}{T_{(N)}}]$
	6.6	18	85.7142	1.8698	
	6.6	19	90.4761	2.3017	$\sqrt{(area)_{max(N)}}=a\cdot y_{(N)}+b$
	6.6	20	95.2380	3.0202	
S55C (No. 3)	10	1	4.7619	−1.1133	$\sigma_{wl}=\frac{1.41\cdot(Hv+120)}{(\sqrt{(area)_{max(N)}})^{1/6}}$
	10	2	9.5238	−0.8550	
	11.6	3	14.2857	−0.6657	
	11.6	4	19.0476	−0.5057	
	11.6	5	23.8095	−0.3612	
	13.3	6	28.5714	−0.2253	
	13.3	7	33.3333	−0.0940	
	13.3	8	38.0952	0.0355	
	13.3	9	42.8571	0.1657	
	13.3	10	47.6190	0.2984	
	13.3	11	52.3809	0.4359	
	16.7	12	57.1428	0.5805	
	16.7	13	61.9047	0.7348	
	16.7	14	66.6666	0.9027	
	18.3	15	71.4285	1.0892	
	19.2	16	76.1904	1.3021	
	20.5	17	80.9523	1.5544	
	21.6	18	85.7142	1.8698	
	21.6	19	90.4761	2.3017	
	24.9	20	95.2380	3.0202	

HSS-Co (No. 3)	a=0.8807, b=4.5939, h=5.055(μm) V_0=2.325E−5(mm^3) $T_{(1)}$=10134193.55, $y_{(1)}$=16.1314 $\sqrt{(area)_{max(1)}}$=18.8(μm)
S55C (No. 3)	a=3.858, b=13.5206, h=15.540(μm) V_0=6.402E−4(mm^3) $T_{(1)}$=368041.23, $y_{(1)}$=12.8159 $\sqrt{(area)_{max(1)}}$=62.96(μm)

* F_j: Cumulative distribution function (%)
y_j: Reduced variables
T : Reflexive time
S_0 : Examined area (mm^2)
d : Specimen diameter (mm)
l : Length in the smooth part of specimen (mm)
N : No. of specimens
n : No. of SEM photos

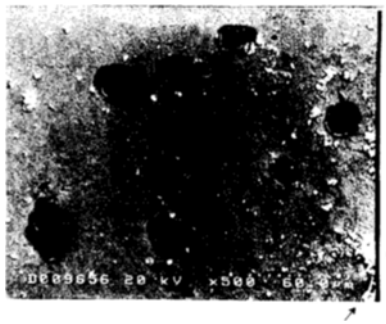

Fig. 3 SEM micrograph showing typical spheroidal cavities in S55C (×500)

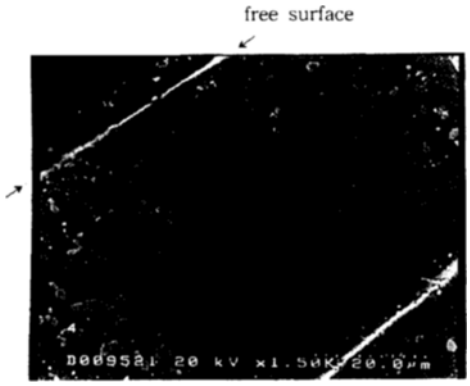

Fig. 4 SEM micrograph showing the structure consisting of tiny spheroidal and some larger alloy carbide particles in a matrix of HSS-Co (×1500)

Figure 4 has shown the structure of HSS-Co consisting of tiny spheroidal and some larger alloy carbide particles in a matrix. The $\sqrt{(area)_{max}}$ of HSS-Co also can be measured by the same procedures as those in S55C. Table 4 exemplifies the details of the procedures in order to get the $\sqrt{(area)_{max}}$ for the HSS-Co (No. 3) and S55C (No. 3) specimens. Furthermore, the obtained values can be plotted on the graph sheet of Weibull distribution type representing the cumulative frequency, and the $\sqrt{(area)_{max}}$ also could be gotten by the same data as those in Table 4 (Murakami, 1993).

3.2 Relationship between $\sqrt{(area)_{max}}$ and N_f

Figure 5 shows the relationship between $\sqrt{(area)_{max}}$ obtained just like Figs. 3 and 4 and

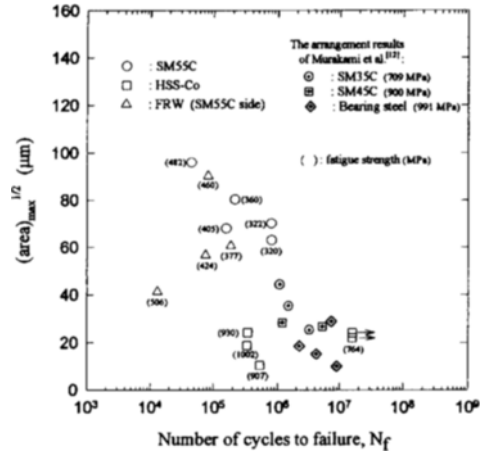

Fig. 5 Relationship between $(area)_{max}^{1/2}$ and N_f

the number of cycles to failure, N_f of the specimen fractured from a surface or a subsurface inclusion. Even though the applied fatigue strengths have a big difference in the same material, the fatigue lives of these materials show an inverse dependence on the size of inclusions. Also the scatter is due to the difference of experimental applied stress. Although the degree of this dependence is vague, the data in this figure show a trend. That is, it was concluded that the larger the value of $\sqrt{(area)_{max}}$, the shorter the fatigue life, N_f. After all, this figure indirectly verifies the usefulness of the geometrical parameter of $\sqrt{(area)_{max}}$. Further, the data of FRW are conformable with those of S55C, resulting in a superiority of the joint performance of FRW. The present results have shown a similar tendency to the previous works of Murakami et al.(1993) that have experimented with a constant applied fatigue strength in a certain material.

3.3 Relationship between fatigue strength and Vickers hardness

For the $\sqrt{(area)_{max}}$, the Eq. (2) is available for predicting the lower limit of fatigue strength for all the specimens (N=4 or 5). An attempt to relate nonmetallic inclusion size $\sqrt{(area)_{max}}$ and practical application parameter Hv to the lower limit of fatigue strength σ_{w1} was made as shown in Fig. 6. Table 5 represents the details of measur-

Table 5 Summary of measurement results

Materials	Smooth specimen No.	Hv	$\sqrt{(area)_{max,j}}$ (μm)	ΔK_{th} (MPa$\sqrt{m}$)	σ_{wl} (MPa)	$\Delta K_{th}/(Hv+120)$	$\sigma_{wl}/(Hv+120)$
HSS-Co	1	1053	24.1	11.18	973	0.0095	0.8295
	1	1053	22.0	10.85	987	0.0092	0.8418
	2	969	10.4	7.84	1038	0.0072	0.95344
	3	1022	18.8	10.02	987	0.0087	0.86467
	4	918	24.3	9.92	860	0.0096	0.82851
S55C	1	249	95.9	5.57	243.2	0.0151	0.65907
	2	250	–	–	–	–	–
	3	251	62.96	4.87	262.3	0.0131	0.70692
	4	233	68.0	4.75	246.4	0.0135	0.69801
	5	250	80.3	5.27	251.2	0.0142	0.67892
	6	261	70.1	5.18	264.6	0.0136	0.69449
FRW (S55C side)	1	268	–	–	–	–	–
	2	244	41.26	4.15	276	0.0114	0.75824
	3	268	56.67	4.91	279	0.0126	0.71943
	4	266	60.63	5.00	274	0.0129	0.71138
	5	307	–	–	–	–	–
	6	287	90.17	6.02	271	0.0148	0.66585

* FRW : Friction welded specimen
Hv : Vickers hardness [Kg_f/mm^2]
$\sqrt{(area)_{max,j}}$: Square root of maximum inclusion size for each specimen [μm]
ΔK_{th} : Threshold stress intensity factor range [MPa$\sqrt{m}$]
σ_{wl} : The lower limit of fatigue strength predicted by Eq. (2) [MPa]

Table 6 The estimated values of $\sqrt{(area)_{max,j}}$ and σ_{wl}

Materials	Vickers hardness Hv	Examined area S_0(mm^2)	Number of specimins N	$\sqrt{(area)_{max,j}}$ (μm)	Lower fatigue limit σ_{wl}(MPa)
HSS-Co	1003	0.0046	5	21.5	950
S55C	249	0.0412	5	83.7	249
FRW (S55C side)	266	0.0412	4	67.9	269

* Hv: The average values of measured specimens

ement results. Three kinds of lines indicate the lower limit of fatigue strength for individual specimen as shown in Table 6. This is compared with the earlier results evaluated by other investigators (Murakami, 1993; Murakami et al., 1991 and Larsson et al., 1991)

If we look at the lines for S55C and the FRW materials there are almost no differences in the lower limit of fatigue strength, σ_{wl}. These may be regarded as the reasons why it has been suggested that the application of the most influential parameters governing the friction welding performance promoted the mechanical properties of the weld zone (Suh et al., 1995a). Thus, in the optimum welding conditions of Table 2, the heat affected zone (HAZ) of the friction welded interface

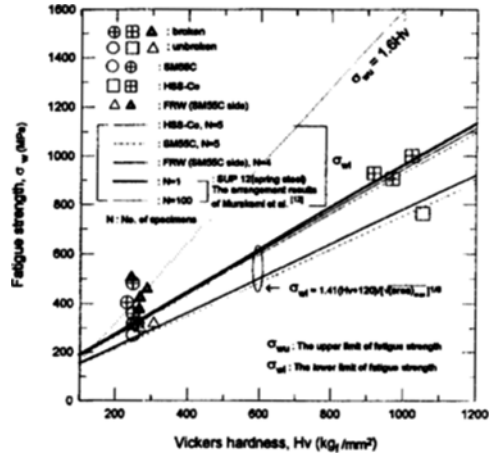

Fig. 6 Comparison of the predicted lower limit of fatigue strength with experimental results

(FRWI) was quite narrow (Suh et al., 1995a). In comparison of the predicted lower limit of fatigue strength with experimental results, it appeared that some satisfactory conclusions could be drawn from these predictions of σ_{wl} according to the $\sqrt{(area)_{max}}$. This figure provides that the size control of nonmetallic inclusions has an importance concerning the balance of fatigue strength and manufacturing economy.

For empirically expected upper limit of the fatigue strength σ_{ul}, a good correlation between the rotary bending fatigue strength σ_0 of smooth specimens and the Vickers hardness Hv for medium strength steels is well known by the formula Eq. (4)(Murakami et al., 1987).

$$\sigma_0 = 1.6H_V \pm 0.1H_V, \text{ for } H_V < 400 \quad (4)$$

where σ_0 and Hv are measured in MPa and kg_f/mm^2.

For Hv>400, this formula is not consistent with their data and could be decreased in a large scatter (Iwakura et al., 1988).

3.4 Relationship between σ_{wl} and $\sqrt{(area)_{max}}$

Figure 7 shows the relationship between $\sigma_{wl}/(Hv+120)$ and $\sqrt{(area)_{max}}$. Analysis of the size of the present largest inclusions indicated that a decreasing ratio of $\sigma_{wl}/(Hv+120)$ was associated with increasing of inclusion size. Although three kinds of specimens were adopted, the data

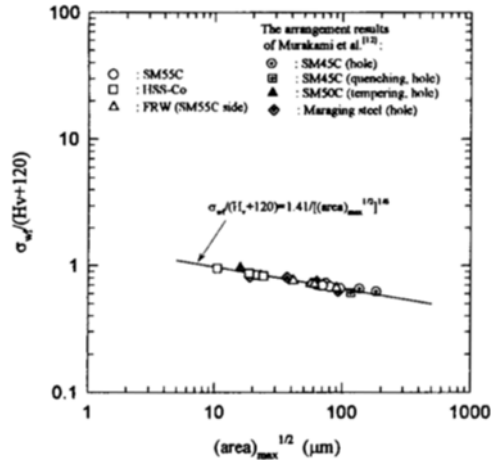

Fig. 7 Relationship between $\sigma_{w1}/(Hv + 120)$ and $(area)_{max}^{1/2}$ for nonmetallic inclusions in smooth specimens

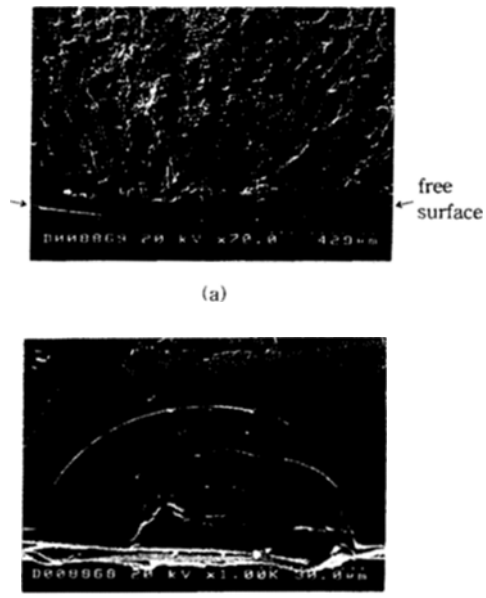

Fig. 8 SEM fractographs of fatigue crack initiation site in FRW material (No. 4, S55C side, $\sigma_w = 377$ MPa, $N_f = 1.85 \times 10^5$cycles)

obtained from all specimens indicated a trend providing any possiblility of correlation considerably as shown in Eq. (5);

$$\sigma_{w_1}/(Hv+120) = 1.41/(\sqrt{(area)_{max}})^{1/6} \quad (5)$$

They showed a trend of increasing failure rate as increasing inclusion category. The effects of natural defects for fatigue strengths of the unnotched specimens obtained in this study compared with the results of Murakami et al.(1993) that have investigated the correlation between $\sigma_{w_1}/(Hv + 120)$ and $\sqrt{(area)_{max}}$ to study the effects of small artificial defects for the fatigue strengths of several metals. Thus, the quantitative evaluation of natural defects on the smooth specimens can be lead to a successful prediction of the fatigue strength.

3.5 Fractographic analysis

Fractographic analysis of the fatigue fractured surfaces provides an important information pertaining to fracture behavior of the specimen. In a crack propagation study recently being conducted by the present authors (Suh et al., 1995a and 1995b) on HSS-Co, S55C and the friction welded materials, the role of nonmetallic inclusions in the fracture process has been observed. The fatigue fractures of the materials were associated primarily with the inclusions located at the outer periphery of the specimen (Figs. 8 and 9) in this study.

The separation of inclusion-matrix interface is evident from the cavities surrounding the particles on the fracture surface. Figures 8 and 9 exemplify the roles of surface and subsurface inclusions in the fatigue failures of FRW (fractured on S55C side) and HSS-Co smooth specimens, identified by SEM fractograph. It is also of interest to note that the enlarged cavities around the inclusion agrees with the apparent fracture nucleating cracks.

Figure 9 represents the Si inclusion exhibited a distinct size of about 21μm and 17μm in a depth and circumferential direction, respectively. It was also confirmed that the fatigue crack was initiated from the nonmetallic inclusion located primarily at the outer periphery of the specimens. Therefore, the existence of inclusion is associated mainly with the crack initiation and propagation due to its stress concentration.

As shown in Fig. 10, EDS compositional analysis for HSS-Co specimen in Fig. 9 revealed the

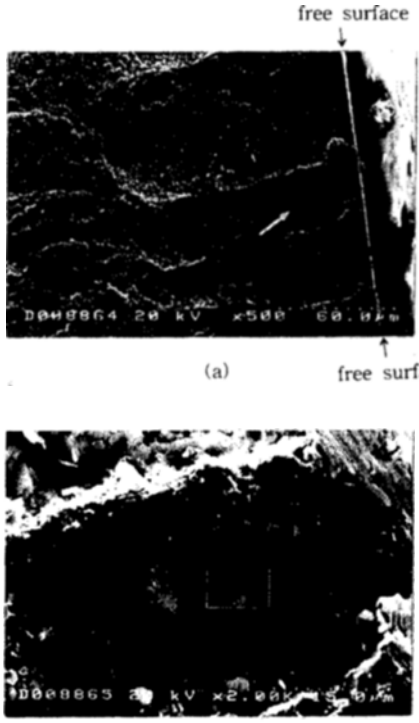

Fig. 9 SEM fractographs showing Si inclusion at the fatigue crack initiation site in HSS-Co(No. 3, $\sigma_w = 1002.3$MPa, $N_f = 3.35 \times 10^5$cycles)

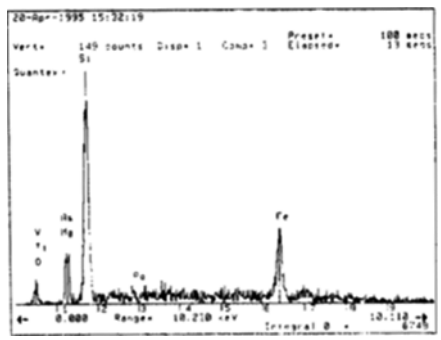

Fig. 10 EDS compositional analysis for HSS-Co specimen in Fig. 9(b)

presence of spherical Si inclusion with a strong peak. This represents the results that fatigue fracture of the material is related mainly with the inclusions located at the outer periphery of the specimen.

3.6 Threshold behavior in fatigue

The threshold value ΔK_{th} of the stress intensity factor for crack propagation has been examined. In most structural alloys the classical Stage I crack initiation mechanism is not observed, and fatigue crack initiation is found to occur at a defect, cavity or nonmetallic inclusion. Each nonmetallic inclusion has an effective stress concentration factor that depends on its dimensions and properties. During cyclic loading, the threshold value ΔK_{th} of the stress intensity factor for a cracked specimen is the limiting value, below which crack propagation is not observed to occur in an infinite number of cycles.

Some experimental results have been obtained on the effect of nonmetallic inclusions with the geometrical parameter $\sqrt{(area)_{max}}$ for various materials (Murakami et al., 1983 and 1987; Murakami, 1989, 1993; and Larsson et al., 1991). The ΔK_{th} is expressed as a unique function of $\sqrt{(area)_{max}}$ of the nonmetallic inclusions, and is estimated using the results of the threshold stress intensity factor range suggested by Eq. (6).

$$\Delta K_{th} = 3.3 \times 10^{-3} (Hv + 120) (\sqrt{(area)_{max}})^{1/3} \quad (6)$$

where ΔK_{th} is measured in MPa • $\sqrt{m}$.

It is assumed that a crack propagation is controlled by the stress intensity threshold value.

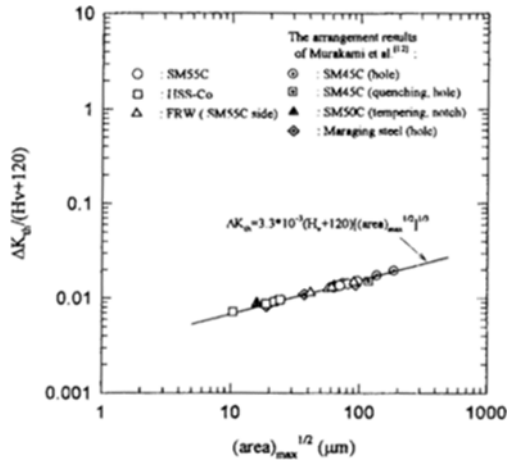

Fig. 11 Relationship between $\Delta K_{th}/(Hv+120)$ and $(area)_{max}^{1/2}$ for nonmetallic inclusions in smooth specimens

Figure 11 has shown that there is a relation between the $\Delta K_{th}/(Hv+120)$ and the maximum inclusion size of $\sqrt{(area)_{max}}$. These results indicate, when the $\sqrt{(area)_{max}}$ is increased by variations in the microstructure, the value of ΔK_{th} is gradually increased with a slope. This would indicate that inclusions play a significant role in mechanism of fatigue crack propagation. And the data represent that there is a consistent change of ΔK_{th} with the $\sqrt{(area)_{max}}$ of inclusion size for examined materials. The consistency of two kinds of data (S55C and FRW) shown in Figs. 7 and 11 functions as a certain evidence supporting a good metallic bond between HSS-Co and S55C. These are compared with the results of the previous studies of other researchers as shown in Fig. 11.

4. Conclusions

The effect of the inclusion size on the fatigue strength was clearly explained from an understanding of the concept of the fatigue limit. For materials such as S55C, HSS-Co and the FRW materials steels which fractured from inclusions or natural defects, the fatigue limit is typically determined by the threshold condition of the crack emanating from nonmetallic inclusions.

In this study, the prediction equation of fatigue strength was applied to the data obtained from fatigue tests and fractographic analysis, and the effect of nonmetallic inclusion size was quantitatively analyzed. The key conclusions are as follows:

(1) The lower limit of fatigue strength, σ_{wl} is uniquely able to be determined from the value of $\sqrt{(area)_{max}}$ in the unnotched smooth specimens of S55C, HSS-Co and FRW materials. The σ_{wl} of the FRW material in the optimum welding conditions is made a good agreement with that of the weaker material, resulting in a superiority of the joint performance of FRW.

(2) An attempt to relate $\sqrt{(area)_{max}}$ and practical application parameter Hv to the σ_{wl} in 3 kinds of the specimens turns out to be very useful and to be in a good agreement with the experimental results. Thus, the quantitative evaluation on the effects of natural defects in the unnotched specimens can be lead to a successful prediction of the fatigue strength.

(3) Assuming a crack propagation is controlled by stress intensity threshold values ΔK_{th}, the relation between ΔK_{th} and $\sqrt{(area)_{max}}$ indicates that inclusions play a significant role in mechanisms of fatigue crack propagation.

(4) From the SEM fractographs, it was confirmed that fatigue crack was initiated from the nonmetallic inclusion located primarily at the outer periphery of the specimens.

(5) The previous characteristics implicitly show that the size control of nonmetallic inclusions is important in the steel-making process or machine components.

References

Atkinson, M., 1960, "The Influence of Nonmetallic Inclusions on the Fatigue Properties of Ultra-High-Tensile Steels," *J. of the Iron and Steel Institute,* 195, pp. 64~75.

De Kazinczy, F., 1970, "Effect of Small Defects on the Fatigue Properties of Medium-Strength Cast Steel," *J. of the Iron and Steel Institute,* 208, pp. 851~855.

Dieter, G. E., 1976, *Mechanical Metallurgy,* 2nd edn., McGraw-Hill, New York, p. 442.

Fowler, G. J., 1979, "The Influence of Non-Metallic Inclusions on the Threshold Behavior in Fatigue," *Materials Science and Engineering,* 39, pp. 121~126.

Ineson, E., Clayton-Cave, J. and Taylor, R. J., 1956, "Variation in Fatigue Properties over Individual Casts of Steel-Part 1," *J. of the Iron and Steel Institute,* 184, pp. 178~185.

Iwakura, S., Shimizu, M. and Kawasaki, K., 1988, "Effect of Toughness and Inclusion on Fatigue Strength of High Strength Steel," *Trans. of JSME,* 54-506, pp. 1826~1830.

Lankford, J., 1977, "Initiation and Early Growth of Fatigue Cracks in High Strength Steel," *Engineering Fracture Mechanics,* Vol. 9, pp. 617~624.

Larsson, M., Melander, A., Blom, R. and Pres-

ton, S., 1991, "Effects of Shot Peening on Bending Fatigue Strength of Spring Steel SS 2090," *Materials Science and Technology,* Vol. 7, pp. 998~1004.

Murakami, Y., Kawakami, K. and Duckworth, W. E., 1991, "Quantitative Evaluation of Effects of Shape and Size of Artificially Introduced Alumina Particles on the Fatigue Strength of 1. 5Ni-Cr-Mo(En24) Steel," *Int. J. Fatigue,* 13-6, pp. 489~499.

Murakami, Y. and Usuki, H., 1989a, "Prediction of Fatigue Strength of High-Strength Steels Based on Statistical Evaluation of Inclusion Size," *Trans. of JSME,* 55-510, pp. 213~221.

Murakami, Y., Kodama, S. and Konuma, S., 1987, "Quantitative Evaluation of Effects of Nonmetallic Inclusions on Fatigue Strength of High Strength Steel," *Trans. of JSME,* 54-500, pp. 688~696.

Murakami, Y., Uemura, Y. and Kawakami, K., 1989b, "Some Problems in the Application of Statistics of Extreme Values to Estimation of the maximum Size of Nonmetallic Inclusions in Metals," *Trans. of JSME,* 55-509, pp. 58~62.

Murakami, Y., 1989, "Quantitative Evaluation of Effects of Defects and Non-metallic Inclusions on Fatigue Strength of Metals," *Iron and Steel,* Japan, 75-8, pp. 1267~1277.

Murakami, Y., 1993, *Metal Fatigue*: Effects of Small Defects and Nonmetallic Inclusions, Yokendo Ltd., Tokyo, pp. 54~72, 156~177, 233 ~250.

Murakami, Y., Kobayashi, M., Makino, T., Toriyama, T., Kurihara, Y., Takasaki, S. and Ebara, R., 1991, "Quantitative Evaluation of the Factors Influencing Fatigue Strength of Spring Steels," *Trans. of JSME,* 57-542, pp. 2305 ~2313.

Murakami, Y. and Nemat-Nasser, S., 1983, "Growth and Stability of Interacting Surface Flaws of Arbitrary Shape," *Engineering Fracture Mechanics,* Vol. 17, No. 3, pp. 193~210.

Suh, C. M., Suh, D. Y. and Lee, D. J., 1995a, "A Study on Fatigue Strength in the Friction Welded Joints of HSS-Co to SM55C Carbon Steel(I)," *Trans. of KSME,* 19-4, pp. 918~928.

Suh, C. M., Suh, D. Y. and Lee, D. J., 1995b, "A Study on Fatigue Strength in the Friction Welded Joints of HSS-Co to SM55C Carbon Steel(II)," *Trans. of KSME,* 19-4, pp. 929 ~940.

Suh, C. M., 1994, *Mechanical Materials,* Wonchang Publishing Co., Korea, p. 190.

Thornton, P. A., 1971, "The Influence of Nonmetallic Inclusions on the Mechanical Properties of Steel: A Review," *J. of Materials Science,* 6, pp. 347~356.

Toriyama, T., Murakami, Y. and Makino, T., 1991, "Database of Nonmetallic Inclusions and Its Application to the Fatigue Strength Prediction Method of High Strength Steels," *J. of Material Science,* 40-458, pp. 1497~1503.

Uemura, Y. and Murakami, Y., 1990, "A Numerical Simulation of Evaluating the Maximum Size of Inclusions to Examine the Validity of the Metallographic Determination of the Maximum Size of Inclusions," *Trans. of JSME,* 56 -521, pp. 162~167.